Levenberg-Marquardt Based Prediction Models for Slabs with Magnesium Sacrificial Anodes Subjected to Chloride Ingress

Y. I. Murthy[1,*] and S. Kumar[2]

[1]*Assistant Professor, Department of Civil Engineering, Jaypee University of Engineering and Technology, Guna, India*
[2]*B. Tech. (third year student), Department of Civil Engineering, Jaypee University of Engineering and Technology, Guna, India*
Corresponding author: yogesh.murthy@juet.ac.in

Received 23/11/2023; accepted 18/04/2024
https://doi.org/10.4152/pea.2026440101

Abstract
This work focused on developing prediction models using ANN, in order to forecast the long-term performance of reinforcements in concrete slabs containing pure Mg anodes, and subjected to Cl^- ingress. The experimental set-up consisted of two built RCC slabs with 1000 x 1000 x 100 mm. Slab #1 was cast with 3.5% NaCl by cement weight. Slab #2 was cast without NaCl. Considered input parameters were the distance of the anode from the point under consideration in x and y-axes, T, RH and concrete age in days. HCP values concerning SCE were considered output. Experimental values consisted of 80 HCP per slab/day. These were collected for 270 days, in order to generate the prediction model. The learning heuristic used LM supervised learning in feed-forward. A two-layer feed-forward network, with ten hidden sigmoid neurons and trained linear output neurons, was employed. The network architecture [5-10-1] and ten neurons in the hidden layer were used for all prediction models. The accuracy level of results obtained with LM was above 97%.

Keywords: ANN model; Cl-induced corrosion; HCP; SA from Mg.

Introduction[•]

RCC is, undoubtedly, one of the most versatile materials used in the construction industry. The concrete in RCC provides a very high compressive strength, is highly durable and can take complex shapes. Steel reinforcement embedded in concrete provides the required tensile and flexural strength. Thus, RCC is robust concerning strength characteristics and durability in general prevailing conditions. However, since free Cl^-, carbonates, sulfates and other ionic materials cause steel corrosion [1], they affect its structural performance. Among these ions, Cl^- is the most

[•]The abbreviations list is in pages 12-13.

detrimental substance affecting RCC structures structural performance, especially those exposed to the marine atmosphere.

In general, the pH of concrete is approx. 13. In such a highly alkaline atmosphere, a weak protective layer of Fe_2O_3 is formed, which acts as a passivating coating and protects steel from corrosion. The ingress of Cl^- from the atmosphere, and the subsequent reaction of these ions with water in concrete pores causes HCl formation, which results in a pH reduction. At a threshold Ct of Cl^-, as reported by [2], the depassivation of the protective thin oxide film of steel reinforcement is initiated. At this stage, the corrosion of reinforcements also takes place, subsequently reducing the cross-sectional area of struts, and decreasing the bonds with the surrounding concrete. In addition, as shown in Fig. 1, the final product of corrosion occupies a volume that is more than six times that of the uncorroded reinforcement [1]. This causes spalling of adherent concrete, which results in complete exposure of reinforcements to the atmosphere, thereby accelerating the corrosion process.

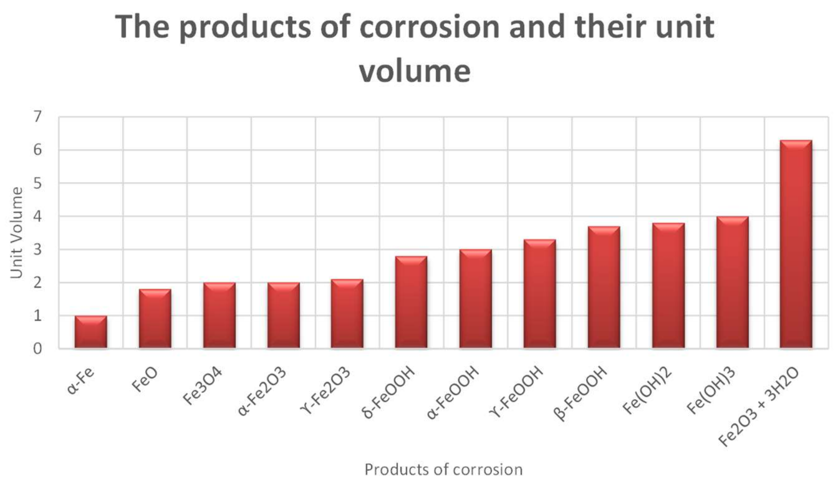

Figure 1: Corrosion products and their unit volume.

The process of Cl-induced corrosion is schematically depicted in Fig. 2. Generally, cement hydration results in the formation of a protective, adherent and passivating $Ca(OH)_2$ film with a high pH value (typically around 13) on the RCC surface [3]. This passive film protects the steel from corrosion for sufficiently long time, due to FeH_2O_2 formation. However, the ingress of free Cl^- and moisture from the atmosphere results in lower pH due to HCl formation, which decreases the protective film passivity [1]. As the ingress of free Cl^- proceeds, pH decreases to around 8, and primary silicates, aluminates and ferrites begin to decompose, thereby lessening the protective film [4]. Several factors affect the onset of reinforcement corrosion through Cl ingress, which include C_3A content, voids, moisture and air content in concrete [5], and non-homogeneous and non-uniform sites in the steel and concrete interface [6].

Thus, in a marine atmosphere, such as in coastal regions, where Ct from Cl^- is extreme, Cl^--induced corrosion is the primary agent causing RCC deterioration. Hence, the development of various novel techniques to mitigate corrosion is an active area of research in the design of offshore structures.

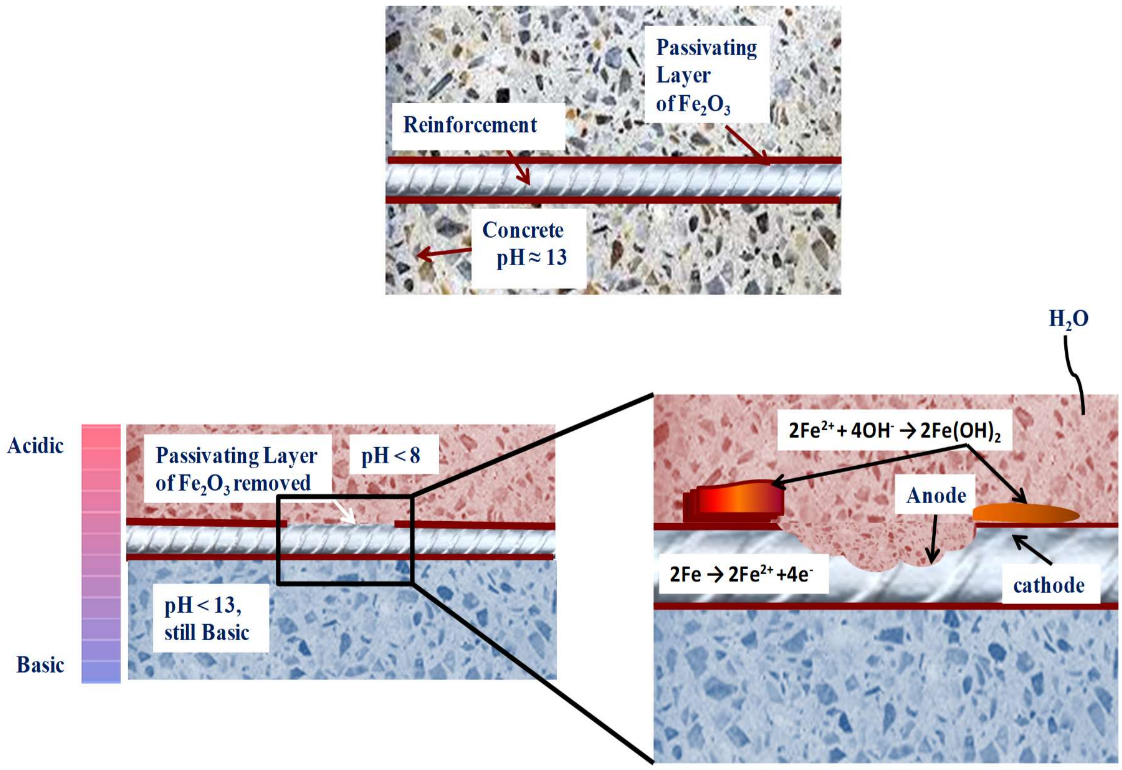

Figure 2: Depassivation of protective oxide film due to Cl^- ingress.

Several techniques for corrosion mitigation are reported by researchers worldwide. These include the use of stainless and galvanized steel [7], corrosion-resistant steel reinforcements [8], corrosion inhibitors [9-13], paints [14], epoxy coatings [15], laminates, reinforced plastics [16] and SA [17]. For marine structures exposed to free Cl^-, the use of SA, also known as the cathodic protection technique, provides a practical and viable solution [18]. This method effectively mitigates the corrosion process, minimizing reinforcements corrosion.

Cathodic protection technique involves the formation of an electrochemical cell in the concrete structure. Metals, such as Mg and its alloys, Al and Zn, with high electronegative E, are used for this purpose. They are connected to the structure's reinforcement, which is rendered cathodic, due to its lower negative electrochemical E. The pore solution which is available in concrete acts as electrolyte. The metals, being anodic, interact with ions, and are rapidly consumed, hence, the name sacrificial anode (Fig. 3). Mg and its alloys are the most commonly used SA, since they possess high electronegative E (2.34 V). Extensive literature on experimental investigations involving corrosion mitigation by Mg alloys as SA is available [17, 19, 20-22]. However, in general, such investigations are conducted over a relatively large duration of time, so as to arrive at conclusions. For example, [23] have carried out their experimental work of 42 months on Mg alloy anodes, and have reported a decrease in Cl content with time.

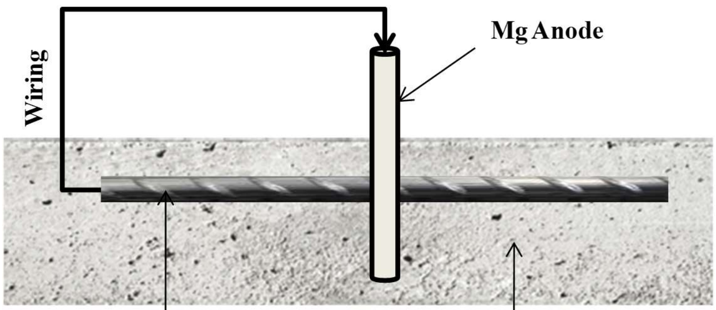

Figure 3: Schematic of cathodic protection of reinforcement.

Due to inherent complexities involved with prolonged experimentation, many researchers have resorted to proposing models that predict corrosion of reinforcements [23-29]. These models are bound to stipulated conditions, and their applications are limited by assumptions such as uniform oxygen Ct distribution and rapid formation of the hydroxide film on steel. Good agreement of these models with experimental data is reported for the given corrosion environment in the system. However, to the author's knowledge, long-term predictions using any of these models for a cathodically protected system have not been not reported. Hence, a measurable model must be developed to predict and analyze the corrosion state of reinforcement in concrete. The most straightforward measure for the corrosion of reinforcement is HCP measurement. These values can be later compared with stipulations laid by international standards [30-33]. Thus, the present work considers the use of HCP measurements, aiming to investigate parametric effects of various environmental factors on HCP values via ANN. It also presents a comparative study of different available ANN algorithms, in terms of regression analysis and effects of T, RH, distance from the anode and age of concrete in days on HCP values.

Scope of this study

The scope of this study covered the comparison of various available algorithms in ANN for concrete slabs containing Cl^-, and subjected to cathodic protection by pure Mg anodes. The significant factors that affect corrosion of reinforcements in such cases, namely, the distance of the point of consideration from the anode, T, RH and concrete age, are considered input parameters. HCP values, which indicate the probability of corrosion, are considered as output. Thus, this study finds major environmental parameters taken over 270 days, to develop prediction models for slabs with Cl^- ingress.

Experimental set-up and materials used

The process of slabs fabrication is shown in Fig. 4. The formwork with dimensions of 1000 x 1000 x 100 mm, as shown in Fig. 4(a), was selected to cast two RCC slabs.

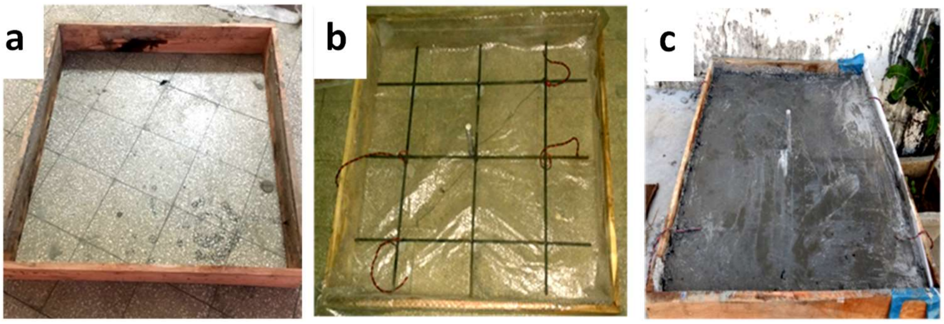

Figure 4: Fabrication steps for concrete slabs: **(a)** formwork; **(b)** reinforcement cage; **(c)** slab after concreting.

A steel reinforcement mat of 10 mm diameter, with a clear cover of 25 mm from all sides and a center to center spacing of 190 mm (Fig. 4(b)), was placed in the formwork. The cover depth was kept constant at 10 mm from the slab top surface, since it has been reported to have significant influence on HCP values [34]. The surface area of the steel reinforcement mat was 1.884 m^2. The reinforcements were treated with a pickling solution, to remove existing corrosion sites, if any. Pure Mg anodes, with diameter and length of 22 and 250 mm, were centrally placed and monolithically cast to complete the electrochemical cell (Fig.4(c)). Insulated copper wires were soldered at the reinforcements ends, and then covered with epoxy. These wires were necessary for measuring HCP values using a SCE. The slabs were cured by covering them with Hessian cloth for 28 days.

HCP test

The schematics for the measurement of HCP value is shown in Fig. 5.

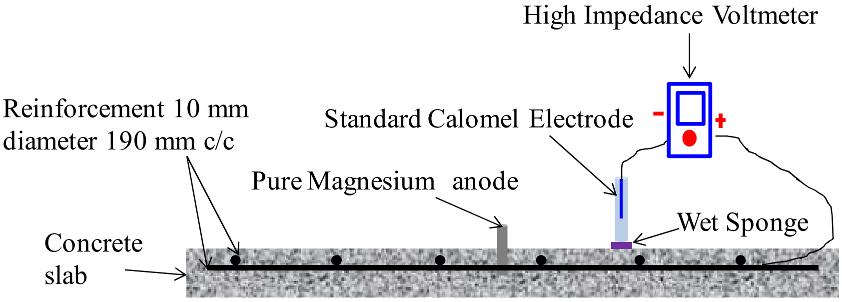

Figure 5: HCP test set-up.

The measurement process involved placing the SCE at the required point, and firmly connecting it to the negative terminal of a high impedance voltmeter. This is a quick and relatively reliable technique to measure E values. ASTM C876-15 [35] provides the correspondence of these measured values and corrosion probability. For example, E values, <-350 mV vs. SCE, have more than 90% probability of corrosion. As per RILEM TC-154's recommendations [36], typical HCP values for reinforcements embedded in concrete, under different situations, are shown in Table 1.

Table 1: Typical HCP values for reinforcements as per RILEM TC-154 [36].

S. no.	Conditions	E values (mV/SCE)
1	Humid, Cl free concrete	-200 to +100
2	Wet, Cl contaminated concrete	-600 to -400
3	Water saturated concrete without oxygen	-1000 to -900
4	Humid, carbonated concrete	-400 to +100
5	Dry, carbonated concrete	0 to +200
6	Dry concrete	0 to +200

However, there are considerable factors mentioned in literature [33], which influence E value readings. These include Cl^- presence, concrete's surface condition and the presence of moisture in it, T and RH, which may shift E reading towards more positive or negative values. In this work, all of these factors were considered.

Materials

Nominal concrete ratio of 1:1.5:3 and water:cement ratio of 0.45 were selected. Slab #1 was cast with 3.5% NaCl by weight of cement. Slab #2 was cast without NaCl. These slabs were constructed using tap water. The casting of both slabs was done on the same day, to create similar conditions.

Cement

OPC 53 grade complying with IS 12269-2013 [37] was used in this work. Physical properties of cement used for fabricating the slabs are shown in Table 2.

Table 2: Physical properties of OPC (53 grade).

Fineness (%)	Le Chatelier soundness(mm)	Specific gravity	Consistency (min.)	Setting time (min)		Compressive Strength (MPa)		
				IST	FS	3 days	7 days	28 days
2.10	8	3.15	30	100	250	28	40	57

Chemical properties following IS 12269-2013 [37] were also evaluated, as shown in Table 3.

Table 3: Chemical properties of OPC (53 grade) in %.

Loss on ignition	CaO	SiO_2	Al_2O_3	Fe_2O_3	MgO	K_2O	Na_2O
3	66.72	18.93	4.57	4.90	0.83	0.45	0.12

Aggregates

Locally available basalt, complying with IS requirements 2386-1963 (Reaffirmed in 1997) [38], of 20 mm down to particle size was used. The particles were thoroughly washed with tap water and dried in the air for 24 h, to remove detrimental substances to concrete, such as silt and dust. The properties of coarse aggregates are mentioned in Table 4. River sand following IS: 383-2016 [39] was used, with particle size distribution shown in Fig. 6.

Table 4: Properties of coarse and fine aggregates.

Coarse aggregate				Fine aggregate			
S. no.	Property	**Values**	**Ref**	**S no.**	**Property**	**Values**	**Ref**
1	Aggregate crushing value %	20.62	[38]	1	Bulk density, kg/m^3	1532	[39]
2	Aggregate impact value%	10.48	[38]	2	Fineness modulus	2.48	
3	Los Angles abrasion value%	12.08	[38]	3	Water absorption%	0.57	
4	Bulk density (kg/m^3)	1623	[40]	4	Specific gravity	2.62	
5	Fineness modulus	6.3	[38]				
6	Water absorption%	0.45					
7	Flakiness index%	6.9					
8	Elongation index%	11.5					
9	Specific gravity	2.66					

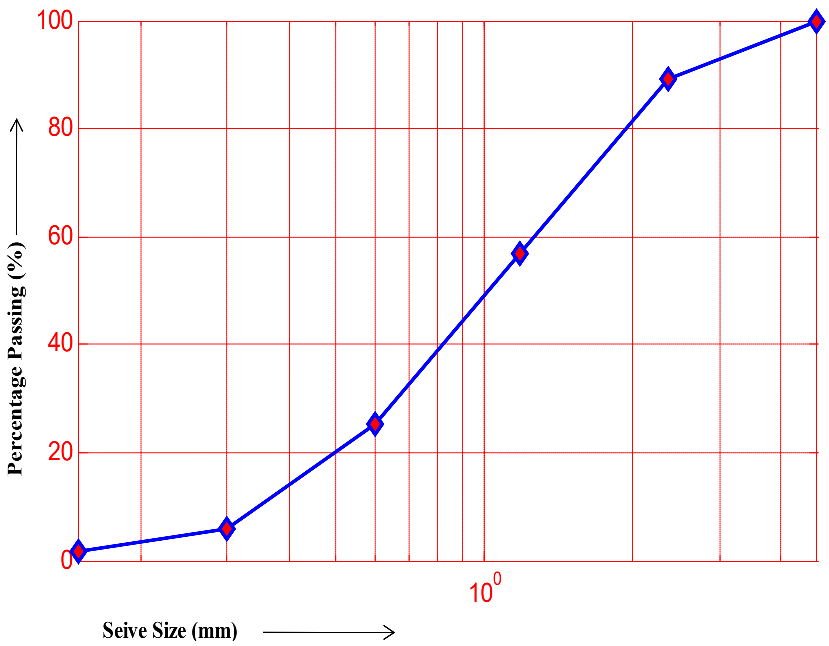

Figure 6: Particle size distribution of sand.

<u>Microstructure of resulting concrete</u>

EDS coupled with SEM was used to identify the morphology of a small concrete segment chipped off after 28 days of curing. The phase compositions were studied using Hitachi S-3400N SEM equipped with EDS. The samples analysis was carried out with a 2 μm probe diameter, 15 kV accelerating V and 50 nA probe current. SEM measurements error was estimated to be about ± two at %. Fig. 7 shows SEM image of concrete.

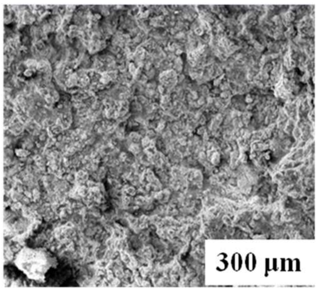

Figure 7: Microstructure of concrete after 28 days of curing.

The image informs that the produced concrete mix is rich and homogeneous. EDS spot analysis performed at several points revealed $Ca(OH)_2$ and C-S-H.

Structuring ANN models

Neural Network Toolbox in MATLAB R2014a was employed to develop an ANN model for predicting HCP values. Training, validation and testing data were randomly divided in 70, 15 and 15% ratio, respectively, as available by default. Feed-forward backpropagation was used to obtain the optimum model, as it decreases the error between model and target outputs by reducing mean square error for a given training set. Sigmoid function was selected as activation function, since it allows for non-linear decision boundaries. ANN architecture used in this model was 5-10-1 (Fig. 8). Other factors were kept constant throughout the experimental study.

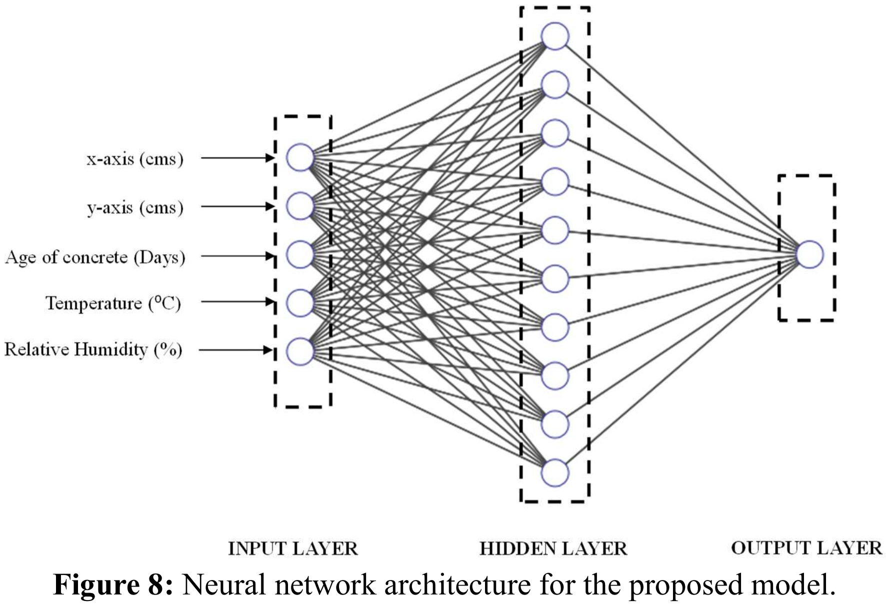

Figure 8: Neural network architecture for the proposed model.

Results and discussion

ANN models to study the effect of distance, T, RH and concrete age on E values

Broadly, there are two basic categories of algorithms: heuristic and standard numerical optimization techniques. While heuristic methods involve variable learning rates by applying momentum and rescaling variables, standard numerical optimization techniques use Newton's methods and conjugate gradient algorithms. In the current work, eight different algorithms were used. These algorithms and their corresponding regression analysis are discussed below.

LM algorithm

Since LM algorithm is a robust optimization method where the second derivative of the Hessian matrix is not required for computation, it is an effective technique for updating weights. The process involves selecting β parameter, with a high onset value, given a set of values of dependent (x_i) and independent variables (Y_i). β final value was sought to minimize S(β) sum of squares, which was herein given by:

$$S(\beta) = \text{argmin}_{\beta}\sum_{i=1}^{m}[y_i - f(x_i, \beta)]^2 \quad (1)$$

The algorithm provided an R-value of 0.99199 for training, 0.9712 for testing, 0.98270 for validation and obtained overall R-value was 0.98696, as shown in Fig. 9.

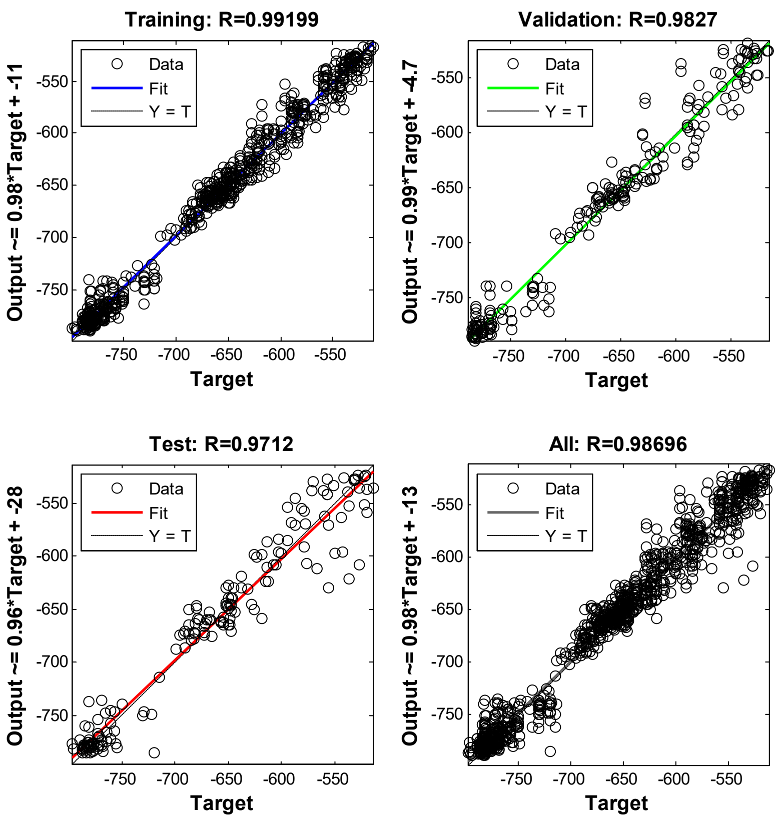

Figure 9: Regression analysis of experimental data using LM algorithm.

Algorithm performance evaluation

Table 5 shows various statistical parameters used to study the fit between the model output and target values. These parameters are COV, CRM, EC, OIMP and RMSE. The formulae used for calculating these parameters and the desired range of values are shown in Table 6. EC highest value, as given by LM, depicts the excellent match between target and forecasted values. These findings suggest that LM algorithm is herein adequate for corrosion prediction of slabs with SA from pure Mg.

Table 5: Statistical parameters and their values for measuring the algorithm performance.

Statistical parameter	Formula	Desired value	LM
RMSE	$\sqrt{\frac{\sum_{i=1}^{n}(a_{p,i}-a_{0,i})^2}{n}}$	As low as possible	0.0019
EC	$1-\frac{\sum_{i=1}^{n}(a_{p,i}-a_{0,i})^2}{\sum_{i=1}^{n}(a_{p,i}-a'_{0,i})^2}$	As close to 1.0 as possible	0.9897
OIMP	$\frac{1}{2}\left[1-\left(\frac{RMSE}{a_{max}-a_{min}}\right)+EC\right]$	As close to 1.0 as possible	0.9978
CRM	$\frac{\left(\sum_{i=1}^{n}a_{p,i}-\sum_{i=1}^{n}a_{0,i}\right)}{\sum_{i=1}^{n}a_{0,i}}$	As close to zero as possible	0.009

Actual vs. predicted values

Values predicted from model #2 shows excellent congruence with the actual values, with the minimum accuracy of prediction being 99.53%, on the 270th day. Results are shown in Fig. 10.

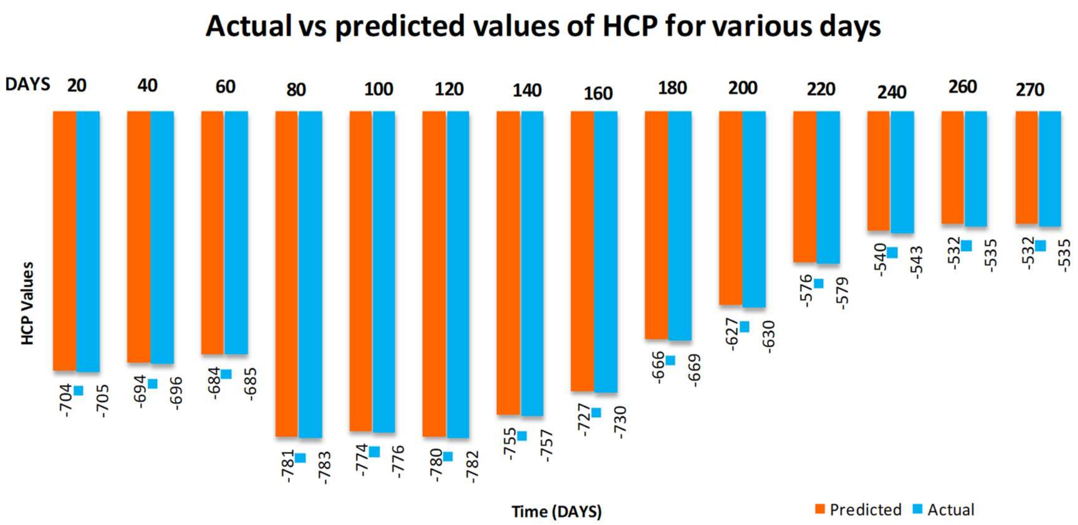

Figure 10: Results of regression analysis using feed-forward backpropagation for slab #2.

This trained ANN model was further validated using data for a slab produced on the same day with equal w/c ratio and materials, but devoid of Cl^-, i.e., slab #2. ANN model revealed an excellent prediction of HCP values (Fig. 11), and demonstrated promising performance, with an overall R-value of 0.97282.

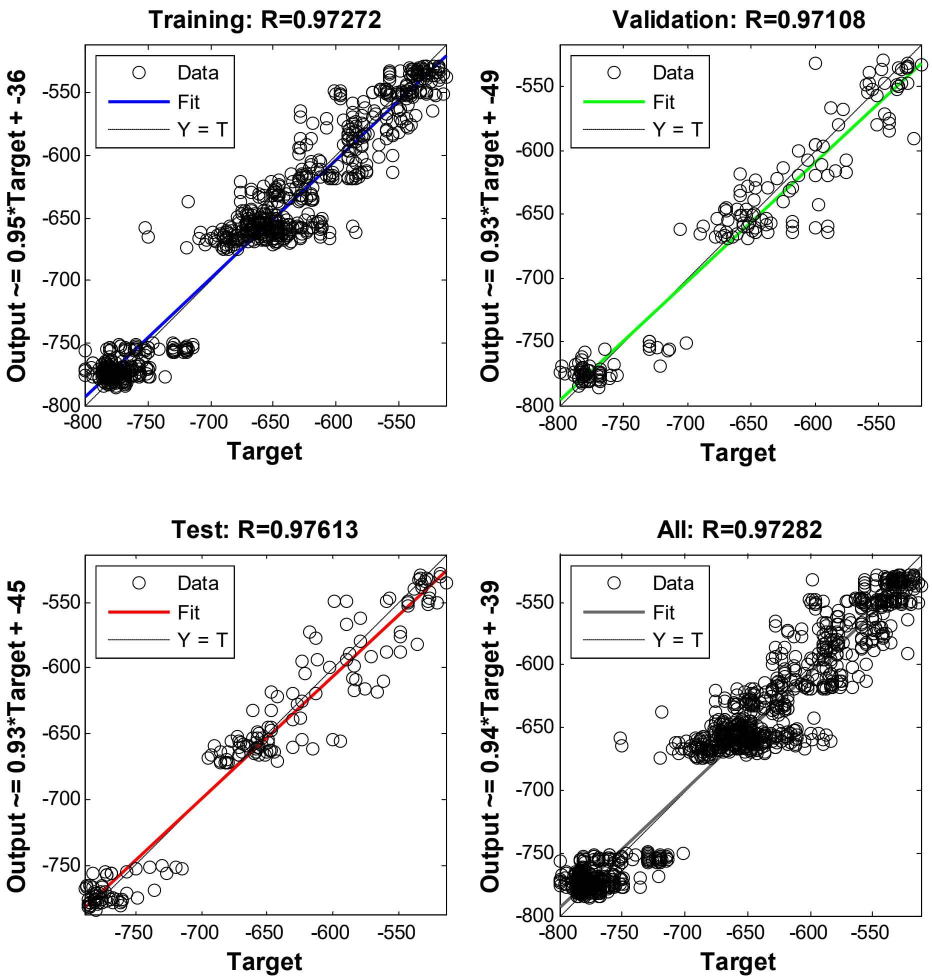

Figure 11: Results of regression analysis using feed-forward backpropagation with hidden layers of ten neurons for slab #2.

Conclusions

Based on experimental data collected for 80 points each, during 270 days, several ANN algorithms were studied to predict the variation in HCP values of RCC slab containing SA from pure Mg subjected to Cl^- ingress. The distance of the point under consideration, from the anode in x and y-axes, T, RH and concrete age in days were considered input parameters. A feed-forward network with hidden sigmoid neurons and linear output neurons trained with various backpropagation algorithms was studied to forecast the prediction model. The network architecture [1, 5, 10] was chosen and the following conclusions were drawn: the prediction of HCP values through an ANN model based on the available experimental data set was excellent. These models can be used to predict future values of HCP and, hence, potential corrosion of embedded reinforcements; COV, CRM, EC, OIMP and RMSE statistical parameters were used to evaluate the algorithm performance; LM provided the maximum proximity to the desired values of statistical parameters. Thus, it is recommended as a feed-forward backpropagation ANN model to estimate HCP values of slabs containing pure Mg anodes; it is herein proposed to develop models that predict the presence of free Cl^-, given HCP value. This will enable the prediction of corrosion sites in RCC slabs.

Acknowledgement
The authors wish to thank the Department of Civil Engineering faculties and staff, at Jaypee University of Engineering and Technology, Guna, for the technical support.

Funding
This research did not receive any specific grant from funding agencies in the public, commercial, or not-for-profit sectors.

Conflict of interest
The authors declare that they have no conflict of interest.

Data availability statement
The data that support the findings of this study are available from the corresponding author, upon reasonable request.

Authors' contributions
Y. I. Murthy: conceptualization; final paper review; results checking. **S. Kumar**: draft preparation; experimentation.

Abbreviations
ANN: artificial neural network
C3A: tricalcium aluminate
$Ca(OH)_2$: calcium hydroxide
Cl^-: chloride ion
COV: coefficient of variation
CRM: coefficient of residual mass
Ct: concentration
E: potential
EC: efficiency coefficient
EDS: energy dispersive spectroscopy
Fe_2O_3: ferric oxide
FeH_2O_2: ferrous hydroxide
HCl: hydrochloric acid

HCP: half-cell potential
LM: Levenberg-Marquardt
NaCl: sodium chloride
OIMP: overall index of model performance
OPC: Ordinary Portland Cement
RCC: reinforced cement concrete
RH: relative humidity
RILEM: International Union of Laboratories and Experts in Construction Materials, Systems and Structures
RMSE: root mean square error
SA: sacrificial anodes
SCE: saturated calomel electrode
SE: secondary electron
SEM: scanning electron microscopy
T: temperature

References

1. Kumar V. Protection of Steel Reinforcement - A Review. Corros Rev. 1998;16(4):317-358. https://doi.org/10.1515/corrrev.1998.16.4.317
2. Silva Campos MDR, Blawert C, Scharnagl N et al. Cathodic protection of mild steel using aluminium-based alloys. Materials (Basel). 2022;(15)4:1301-1313. https://doi.org/10.3390/ma15041301
3. Vu KAT, Stewart MG. Structural reliability of concrete bridges including improved chloride-induced corrosion models. Struct Saf. 2000;(22)4:313-333. https://doi.org/10.1016/S0167-4730(00)00018-7
4. Angst U, Elsener B, Larsen CK et al. Critical chloride content in reinforced concrete - A review. Cem Concr Res. 2009;(39)12:1122-1138. https://doi.org/10.1016/j.cemconres.2009.08.006
5. Angst U. Chloride induced reinforcement corrosion in concrete - Concept of critical chloride content – methods and mechanisms. 2011. URI: http://hdl.handle.net/11250/23672
6. Sergi G, Broomfield J, Davison N. The Principles and Practice of Galvanic Cathodic Protection for Reinforced Concrete Structures. Technical Note 6. Corrosion Prevention Association. 2018:115.
7. Prasad NK, Pathak AS, Kundu S et al. Highly active and efficient hybrid sacrificial anodes based on high p pig iron, Zn and Mg. J Electrochem Soc. 2021;168(11):111504. https://doi.org/10.1149/1945-7111/ac3600
8. Mohamed N, Boulfiza M, Evitts R. Corrosion of carbon steel and corrosion-resistant rebars in concrete structures under chloride ion attack. J Mater Eng Perform. 2013;22(3). https://doi.org/10.1007/s11665-012-0314-0
9. Gurmeet Singh. Corrosion inhibitors. Corr Rev. 2009. https://doi.org/10.1515/corrrev.2009.27.s1.367
10. Söylev TA, Richardson MG. Corrosion inhibitors for steel in concrete: State-of-the-art report. Constr Build Mater. 2008;22(4):609-622. https://doi.org/10.1016/j.conbuildmat.2006.10.013

11. Ormellese M, Berra M, Bolzoni F et al. Corrosion inhibitors for chlorides induced corrosion in reinforced concrete structures. Cem Concr Res. 2006;36(3):536-547. https://doi.org/10.1016/j.cemconres.2005.11.007
12. Elsener B, Angst U. Corrosion inhibitors for reinforced concrete. Sci Technol Concr Admix. 2016:321-339. https://doi.org/10.1016/B978-0-08-100693-1.00014-X
13. Al-Amoudi OSB, Maslehuddin M, Lashari AN et al. Effectiveness of corrosion inhibitors in contaminated concrete. Cem Concr Compos. 2003;25(4-5):439-449. https://doi.org/10.1016/S0958-9465(02)00084-7
14. Dias P, Carneiro C, Andrade L et al. Characterization of a water-based paint for corrosion protection. J Coat Technol Res. 2012;9:365-374. https://doi.org/10.1007/s11998-011-9388-0
15. Dong S, Zhao B, Lin C et al. Corrosion behavior of epoxy/zinc duplex coated rebar embedded in concrete in ocean environment. Constr Build Mater. 2012;28(1):72-78. https://doi.org/10.1016/j.conbuildmat.2011.08.026
16. Ahmad Z, Al-Sulaiman F, Abdul ABJ. Corrosion behavior of carbon reinforced plain-weave laminates. J Reinf Plast Compos. 2004;23(10):1041-1050. https://doi.org/10.1177/0731684404035268
17. Parthiban GT, Bharanidharan K, Dhayanand D et al. Influence of sacrificial cathodic protection on the chloride profile in concrete. Int J Electrochem Sci. 2008;(3)10:1162-1168. https://doi.org/10.1016/S1452-3981(23)15512-X
18. Bertolini L, Gastaldi M, Pedeferri MP et al. Prevention of steel corrosion in concrete exposed to seawater with submerged sacrificial anodes. Corros Sci. 2002;44(7):1497-1513. https://doi.org/10.1016/S0010-938X(01)00168-8
19. Murthy YI, Gandhi S, Kumar A. Corrosion Prevention of Steel Reinforcement in 7.5% NaCl Solution using Pure Magnesium Anode. IOP Conf Ser: Mater Sci Eng. 2017;330:012003. https://doi.org/10.1088/1757-899X/330/1/012003
20. Murthy YI, Gandhi S, Kumar A. Magnesium alloy anodes for corrosion prevention of reinforcements in concrete. Int J Emerg Technol. 2020;11(2):656-661. ISSN No. (Print): 0975-8364. ISSN No. (Online): 2249-3255
21. Wang Z, An X, Wang P et al. Removal of high concentration of chloride ions by electrocoagulation using aluminium electrode. Environ Sci Pollu Res. 2023;(30)17:1-15. https://doi.org/10.1007/s11356-023-25792-1
22. Wu Y, Xu J, Gong W et al. Application of magnesium alloy sacrificial anode for restraining chloride ingress into mortar. Constr Build Mater. 2022;(344):128212. https://doi.org/10.1016/j.conbuildmat.2022.128212
23. Yu B, Yang L, Wu M et al. Practical model for predicting corrosion rate of steel reinforcement in concrete structures. Constr Build Mater. 2014;(54):385-401. https://doi.org/10.1016/j.conbuildmat.2013.12.046
24. Ouzaa K, Oucif C. Numerical model for prediction of corrosion of steel reinforcements in reinforced concrete structures. Undergr Sp. 2019;(4)1:72-77. https://doi.org/10.1016/j.undsp.2018.06.002
25. McMahon ME, Korjenic A, Burns JT et al. Mechanistic Insight into Al-Zn, Mgand Al-Mg-Rich Primer Design for Enhanced Cathodic Prevention on Sensitized Al-Mg Alloys. Corrosion. 2023;(79)6:647-664. https://doi.org/10.5006/4289

26. Hodhod OA, Ahmed HI. Modeling the corrosion initiation time of slag concrete using the artificial neural network. Hous Build Nat Res Cent J. 2014;(10)3:231234. https://doi.org/10.1016/j.hbrcj.2013.12.002
27. Thike PH, Zhao Z, Shi P et al. Significance of artificial neural network analytical models in materials' performance prediction. Bull Mater Sci. 2020;43(1). https://doi.org/10.1007/s12034-020-02154-y
28. Roxas CLC, Lejano BA. An artificial neural network model for the corrosion current density of steel in mortar mixed with seawater. Int J GEOMATE. 2019;(16)56:79-84. https://doi.org/10.21660/2019.56.4585
29. Taffese WZ. Data-driven method for enhanced corrosion assessment of reinforced concrete structures. Univ Turku. 2020. https://doi.org/10.13140/RG.2.2.19695.25766
30. Elsener B. Half-cell potential mapping to assess repair work on RC structure. Constr Build Mater. 2001;15(2-3):133-139. https://doi.org/10.1016/S0950-0618(00)00062-3
31. Leelalerkiet V, Kyung JW, Ohtsu M. et al. Analysis of half-cell potential measurement for corrosion of reinforced concrete. 2004;18(3):155-162. https://doi.org/10.1016/j.conbuildmat.2003.10.004
32. Liu G, Zhang Y, Ni Z et al. Corrosion behavior of steel submitted to chloride and sulphate ions in simulated concrete pore solution. Constr Build Mater. 2016;(115):1-5. https://doi.org/10.1016/j.conbuildmat.2016.03.213
33. Yodsudjai W, Pattarakittam T. Factors influencing half-cell potential measurement and its relationship with corrosion level. Measurement. 2017;104:159-168. https://doi.org/10.1016/j.measurement.2017.03.027
34. Murthy YI. Neural Network Models for the Half-Cell Potential of Reinforced Slabs with Magnesium Sacrificial Anodes Subjected to Chloride Ingress. J Soft Comput Civ Eng. 2024;(8)1:85-106. https://doi.org/10.22115/SCCE.2023.347658.1470
35. ASTM International, Standard test method for corrosion potentials of uncoated reinforcing steel in concrete. ASTM C876 - 15. G01.14. ASTM Int., 2015.
36. Wang L, Gu K, Zhang Y et al. Enhanced struvite generation and separation by magnesium anode electrolysis coupled with cathode electrodeposition. Sci Tot Environ. 2022;804:150101. https://doi.org/10.1016/j.scitotenv.2021.150101
37. Bureau of Indian Standards, IS:12269-2013. Ordinary Portland Cement, 53 grade specification (First Revision). Bur Ind Stand. New Delhi, India, 2013.
38. Bureau of Indian Standards, IS: 2386-1963.Ind Stand. Methods test aggregates Concrete (Part-I to Part-VIII).
39. Bureau of Indian Standards, IS: 383-2016. Ind Stand Specif coarse fine aggregates from Nat sources Concrete. Third Revis. Reaffirmed 2016.